

# Characterization and Optimization of Yb-Doped Photonic-Crystal Fiber Rod Amplifiers Using Spatially Resolved Spectral Interferometry

## Introduction

New Yb-doped photonic-crystal fibers (PCF's) have enabled fiber-based chirped-pulse-amplification (CPA) systems to produce millijoule-level pulses, compressible to femtosecond pulse widths.<sup>1,2</sup> Rigid double-clad fiber rods are commercially available with large effective areas ( $>2300 \mu\text{m}^2$ ) and high pump absorption ( $\sim 30 \text{ dB/m}$  at  $976 \text{ nm}$ ) for efficient amplification in less than a meter of fiber. The combination of large effective areas and short amplifier lengths limits the suppression of higher-order modes (HOM's), however, and these fibers may support several modes in addition to the fundamental. The rigid rod construction reduces the coupling between the weakly guided fundamental and other modes in the fiber. HOM's may be excited when the signal is injected, which is typically done by focusing a free-space beam into the core. Relatively small amounts of HOM that are co-polarized with the fundamental mode can significantly degrade the beam quality and pointing stability because they interfere coherently.<sup>3,4</sup>

This article reports the first application of a recently proposed technique,  $S^2$  imaging,<sup>5,6</sup> to measure the modes of a Yb-doped PCF amplifier at full power. The technique, based on spatially resolved spectral interferometry, can detect small amounts of HOM that beat with the fundamental mode.  $S^2$  imaging measures HOM fields relative to the fundamental mode without requiring *a priori* knowledge of the design of the fiber or its mode content.  $S^2$  imaging provides feedback when optimizing signal injection and is more sensitive than measuring the amplifier gain.

## $S^2$ Imaging

$S^2$  imaging detects HOM content from fringes in the spatially resolved spectra that are sampled across the beam profile. Nicholson *et al.* showed that an HOM's profile and its intensity and phase relative to the fundamental mode can be directly calculated from the spatially dependent fringe visibility.<sup>5</sup> Consider two modes defined by the spectral fields  $E_1(x,y,\omega)$  and  $E_2(x,y,\omega)$ , where  $E_1$  is assumed to be the fundamental mode (such as the  $\text{LP}_{01}$ ) and  $E_2$  is an HOM that is coherent

and co-polarized with  $E_1$ . As  $|E_1|$  is nonzero across the beam,  $E_2$  can be expressed as

$$E_2(x,y,\omega) = \alpha(x,y,\omega)E_1(x,y,\omega), \quad (1)$$

where  $\alpha(x,y,\omega)$  is the relative field amplitude of the HOM at a given position in the beam. It is a complex function:  $|\alpha|\exp(i\phi_\alpha)$ . After propagation with relative group delay,  $\Delta\tau_G$ , the mode fields are related by

$$E_2(x,y,\omega) = \alpha(x,y,\omega)E_1(x,y,\omega)\exp(-i\omega\Delta\tau_G). \quad (2)$$

Spectral interference between the two fields produces a combined spectral intensity of the form

$$\begin{aligned} I(x,y,\omega) &= |E_1(x,y,\omega) + E_2(x,y,\omega)|^2 \\ &= I_1(x,y,\omega) [1 + |\alpha|^2 + 2|\alpha|\cos(\omega\Delta\tau_G - \phi_\alpha)]. \end{aligned} \quad (3)$$

The spectrum contains fringes because of the relative group delay between the modes. Assuming that  $\alpha$  and  $\Delta\tau_G$  are slowly varying functions of frequency and there are several fringes across the spectrum, standard Fourier analysis is used to extract the relative powers of the two modes. The ac sidebands produced by the modal interference have an amplitude relative to the dc peak that is given by

$$f(x,y) = \frac{2|\bar{\alpha}|\exp(-i\phi_\alpha)}{1 + |\alpha|^2}, \quad (4)$$

where  $\bar{\alpha}(x,y)$  is the spectral average of  $\alpha(x,y,\omega)$  that can be calculated directly from  $f(x,y)$ :

$$\bar{\alpha}(x,y) = \frac{1 - \sqrt{1 - 4|f(x,y)|^2}}{2f(x,y)}. \quad (5)$$

The relative power of the HOM to the fundamental is obtained from  $\bar{\alpha}(x,y)$  and the total intensity integrated over the entire spectrum,  $I_T(x,y)$ :

$$P_2/P_1 = \frac{\iint I_2(x,y)dx dy}{\iint I_1(x,y)dx dy} = \frac{\iint I_T |\bar{\alpha}|^2 / (1 + |\bar{\alpha}|^2) dx dy}{\iint I_T / (1 + |\bar{\alpha}|^2) dx dy} \quad (6)$$

Since the  $S^2$  technique is fundamentally interferometric in nature, the relative phase between the modes at a given position in the beam is encoded on the phase of the spectral oscillations at that position. Equation (4) shows that the phase between the modes across the beam,  $\phi_\alpha(x,y)$ , is given by the phase of  $f(x,y)$ . The phase of the fundamental mode does not vary across the beam, so  $\phi_\alpha(x,y)$  represents the phase variation across the HOM. An  $LP_{11}$  mode, for example, has two lobes with a  $\pi$ -phase shift between them, which can be measured using  $S^2$  imaging.<sup>5</sup> Although only one HOM was considered here, multiple HOM's can be imaged simultaneously providing the relative group delays between each HOM and the fundamental mode are sufficiently different that the sidebands are clearly resolved. Reference 6 extends this analysis to cases where (1) the excitation of the HOM's is distributed along the fiber device and (2) the coupling between the modes and their relative group delays is frequency dependent. While this alternate method of analysis is more general, it requires that each HOM

is weak compared to the fundamental mode (relative power less than -15 dB) to ensure  $S^2$  imaging does not underestimate the HOM power.

### Experimental Setup

The experimental setup is shown in Fig. 119.14. The Yb-doped PCF fiber (DC-200/70-PM-Yb-ROD from Crystal Fibre A/S) was a rigid rod (0.8-m  $\times$  1.7-mm diameter) with angle-cleaved end faces ( $4^\circ$ ). The signal core, formed by a hexagonal matrix of air holes, has an effective area of  $2300 \mu\text{m}^2$ , corresponding to a mode-field diameter (MFD) =  $55 \mu\text{m}$  and a numerical aperture (N.A.)  $\approx 0.015$ . Boron-doped stress-applying parts (SAP's) limit propagation to a single linear polarization in the signal wavelength range.<sup>2</sup> The amplifier was pumped at 976 nm using multimode pigtailed diodes. An output power of 16 W at 1055 nm with 16.6 dB of gain was obtained for  $\sim 50$  W of absorbed pump power.

The amplifier output was sampled using a single-mode fiber probe (MFD =  $6 \mu\text{m}$ , N.A. = 0.14) and a fiber-coupled spectrometer (Ocean Optics HR2000+). The beam was attenuated using three uncoated reflections and neutral-density (ND) filters. The PCF end face was imaged onto the fiber probe with  $6\times$  magnification so that the MFD of the probe fiber was less than  $1/50$  of the beam's diameter ( $1/e^2$ ). High-speed actuators (Newport LTA) were used to translate the fiber probe across the beam and the spectrum was measured at each point. The total acquisition time for a scan ( $32 \times 32$ ) was approximately 6 min. The half-wave plate was set to either align the amplifier output with the polarizer or rotate the polarization by  $45^\circ$ . In the first

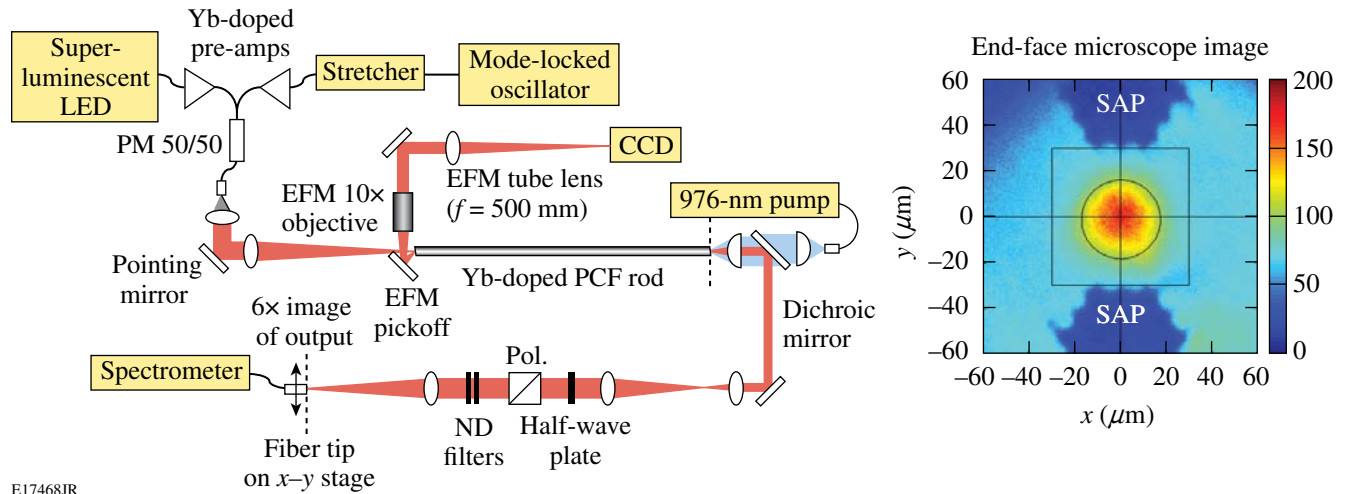


Figure 119.14  
Experimental setup. The EFM image shows signal beam at injection, aligned between the two SAP regions that are backlit by the pump.

case, fringes were produced by HOM's that were co-polarized with the fundamental mode. In the second, fringes could potentially be produced by HOM's that were orthogonally polarized to the fundamental. Thus, the relative polarization state of the HOM to the fundamental was determined by comparing the fringe visibility for both wave-plate settings.

One challenge in applying  $S^2$  imaging to short amplifiers is that the relative group delay between modes is short, resulting in spectral fringes with a long period. A combination of stretched Yb oscillator pulses at 1055 nm and output from a superluminescent light-emitting diode (SLED) at 1035 nm was injected to provide at least four fringes across the spectrum. Each spatially resolved spectrum was first normalized by the spectrum integrated over the beam before Fourier analysis so that the entire wavelength range (1020 to 1060 nm) could be used.

Independent measurements of the signal beam offset at injection were provided using an end-face microscope (EFM) to image the input end of the PCF amplifier. The EFM used a pickoff mirror located a few millimeters from the fiber end and a microscope objective to capture the signal reflection from the angle-cleaved fiber face. In addition, the EFM collected part of the residual pump light exiting the fiber at large angles. Figure 119.14 shows a typical EFM image with signal and pump light present. The pickoff angle exceeded the numerical aperture of pump light guided in the two trapezoidal SAP's; therefore, they appear as dark regions that indicate the location of the signal core. Using standard image-processing techniques, this simple setup can measure signal-to-core overlap at the end face with micron-level precision.

### Experimental Results of $S^2$ Imaging Measurements

Figure 119.15(a) shows the amplified spectrum integrated over the entire beam for the SLED and mode-locked oscillator (ML OSC). Figure 119.15(b) shows two examples of spatially resolved spectra, measured at positions of low- and high-fringe visibility, after normalization by the integrated spectrum. The corresponding Fourier magnitudes are plotted versus group delay in Fig. 119.15(c) and show an interference peak at a group delay of 420 fs/m.

Mode images were extracted using the spatial dependence of 420-fs/m peak. The images are shown in Fig. 119.16 along with a direct charge-coupled-device (CCD) measurement of the beam. The dimensions for all images correspond to the amplifier output before the 6 $\times$  magnification in front of the fiber probe. The modes are the fundamental LP<sub>01</sub> mode and the LP<sub>11</sub> mode, which is aligned with the SAP axis. The LP<sub>11</sub> mode was determined to be co-polarized with the LP<sub>01</sub> mode by rotating the half-wave plate before the polarizer and noting that the fringe visibility remained constant. In principle,  $S^2$  imaging can detect many HOM's from a single scan. In this case only one clear mode was observed, corresponding to the generation of the LP<sub>11</sub> mode at injection into the amplifier. Other modes could be present, such as HOM's generated from scattering from inhomogeneities distributed along the amplifier length. The relative group delay depends on the scattering position, and, therefore, fringes are produced with a range of periods from a minimum value set by the total length of the amplifier to larger values. Detecting HOM's from such distributed coupling is possible<sup>4</sup> but was not feasible given the signal-to-noise ratio of the data.

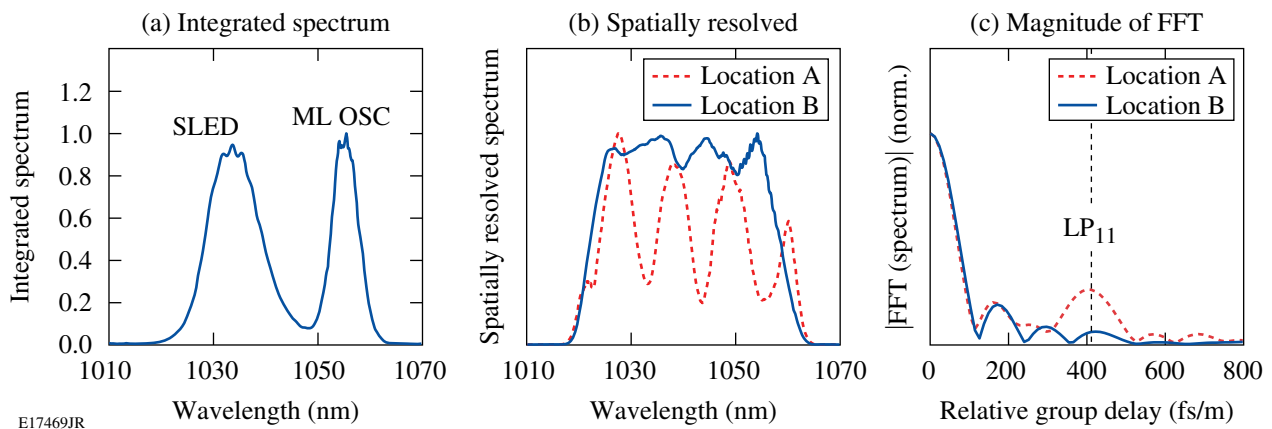


Figure 119.15

(a) Integrated amplified spectrum. (b) Spatially resolved spectra, after normalization with the integrated spectrum, at locations of low- and high-fringe visibility (solid and dashed, respectively). (c) Corresponding Fourier transform magnitudes, with dashed line showing the location of LP<sub>11</sub> signal.

$S^2$  imaging provides a direct measurement of the beam profile at a given wavelength. This method of viewing the data is presented as a sequence of images in Fig. 119.17. The relative

$LP_{11}$  power in this case was  $-13$  dB. As the wavelength changes, the beam centroid moves vertically in the  $y$  direction, along the  $LP_{11}$  axis (see Fig. 119.18). This beam motion is a direct

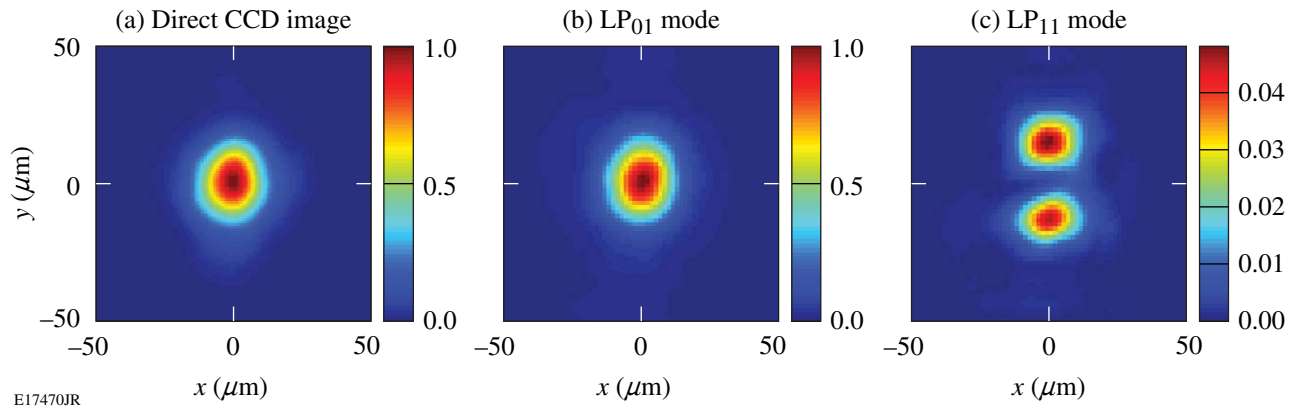


Figure 119.16

(a) Output beam as measured using a 12-bit CCD. [(b), (c)] Modes reconstructed using the  $S^2$  technique.

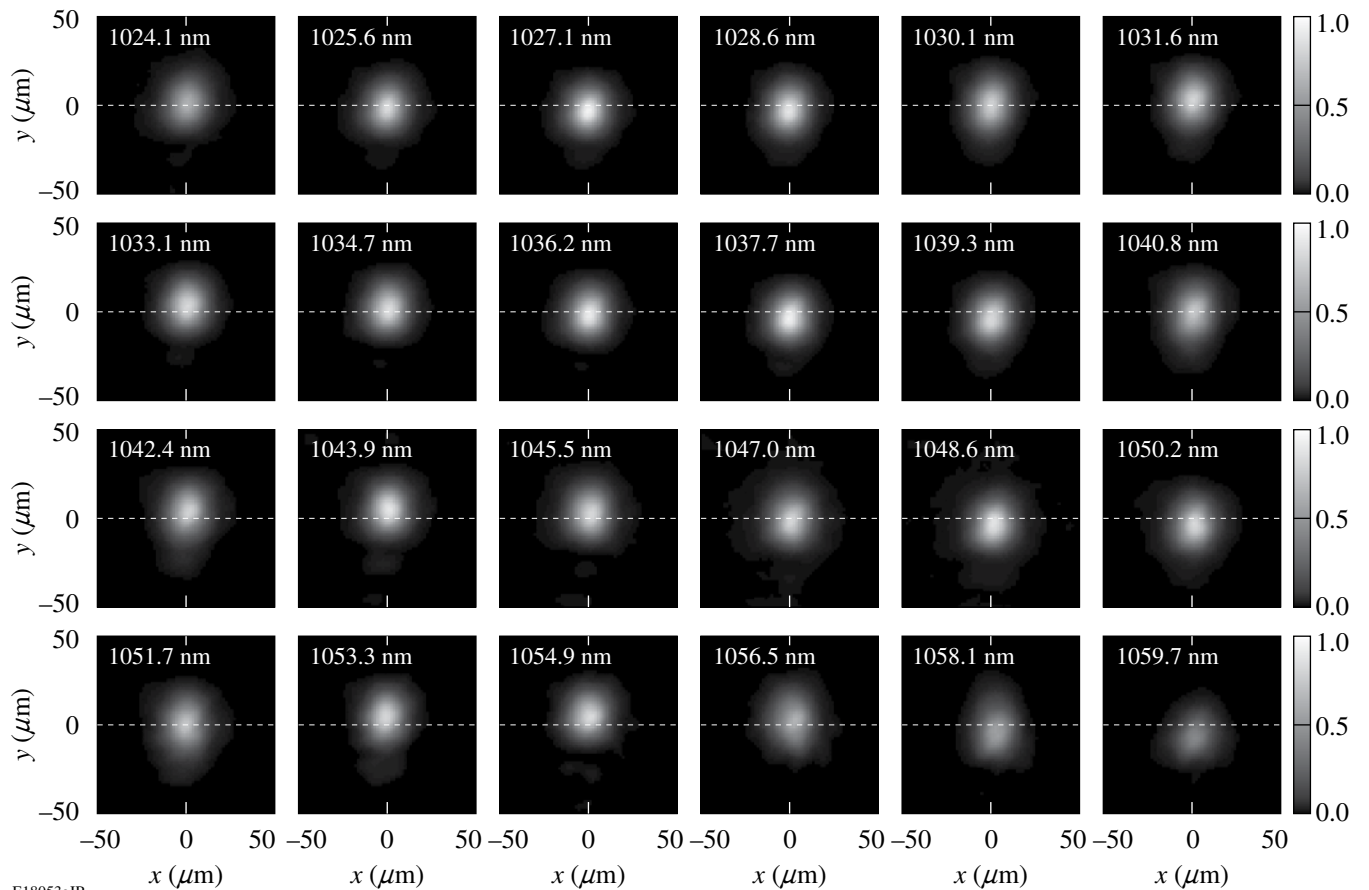


Figure 119.17

Spectrally resolved images that are measured by the  $S^2$  technique. The oscillation of the beam with wavelength in the  $y$  direction is due to the wavelength dependence of the phase between the  $LP_{01}$  and  $LP_{11}$  modes. [Click for animation](#)

consequence of the coherence and co-polarization of the two modes. At wavelengths corresponding to a positive  $y$  centroid, the upper lobe of the  $LP_{11}$  mode interferes constructively with the  $LP_{01}$  mode, and the lower lobe interferes destructively. This oscillation would not be seen if the modes were incoherent or orthogonally polarized.

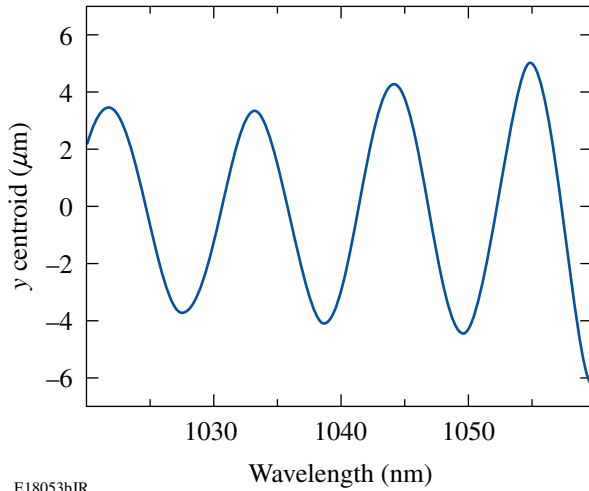


Figure 119.18  
The beam centroid in the  $y$  direction as a function of wavelength.

These observations raise important questions about the impact of HOM's in broadband amplifiers. When the signal bandwidth is much larger than the fringe period, deflection of the beam centroid at each wavelength will average to zero over the full spectrum. Although the integrated beam profile is broadened along the HOM axis, it is relatively insensitive to phase fluctuations between the modes. If the signal bandwidth is less than the fringe period, phase fluctuations significantly alter the integrated beam profile since there is insufficient bandwidth to average out the beam variations at each spectral component. For this amplifier, a Gaussian signal bandwidth equal to single fringe period (FWHM = 11 nm) corresponds to a 150-fs transform-limited pulse. The relative phase of the modes was stable during the  $S^2$  scan (several minutes), in part because the fundamental mode and the HOM propagate along the same length of fiber. Long-term stability will depend on the details of the amplifier's thermal environment and stability of signal injection, so no general conclusions can be drawn from these data.

### Impact of Misalignment at Signal Injection on HOM Content

The impact of misalignment at injection was evaluated by offsetting the beam with the pointing mirror (see Fig. 119.14),

using the EFM to quantify the amount of offset at signal injection, and the  $S^2$  measurements to measure the resulting HOM content. The results are shown in Fig. 119.19. Significant amounts of  $LP_{11}$  were excited when injection was misaligned along the axis of the  $LP_{11}$  mode (the  $y$  axis). This offset direction increases the mode overlap between the input signal beam and one of the lobes of the  $LP_{11}$  mode, producing a larger fraction of the  $LP_{11}$  mode at injection. The power in  $LP_{11}$  was only -13 dB below that for  $LP_{01}$  for a 15- $\mu$ m offset ( $\sim 30\%$  of the MFD). The large misalignment reduced the amplifier gain by only  $\sim 0.5$  dB.

Simulations using a simple step-index model predict that these levels of  $LP_{11}$  can have a small but measurable impact on the amplifier beam's quality. The fiber parameters were chosen to match the MFD and N.A. of the amplifier (core radius  $a =$

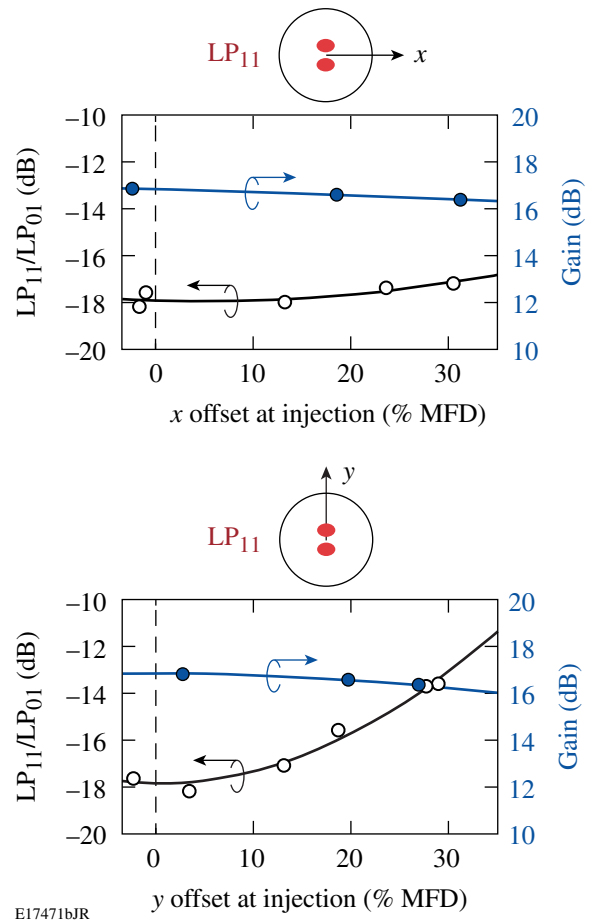


Figure 119.19  
Relative power in  $LP_{11}$  mode versus injection offset. Offset along the (a)  $x$  direction (across SAP axis) and (b) the  $y$  direction (along SAP axis). Also shown is the gain in dB as a function of offset.

28  $\mu\text{m}$ ; index difference  $\Delta = 5.3 \times 10^{-5}$ ) and to set the  $\text{LP}_{11}$  mode close to cutoff ( $V = 2.50$ ). While these calculations did not include the full model for the PCF design or birefringence, some qualitative conclusions can be reached. Figure 119.20 shows the simulated values of beam quality ( $M^2$ ) in the  $x$  and  $y$  directions plotted as a function of the ratio of  $\text{LP}_{11}$  to  $\text{LP}_{01}$  powers, where the  $\text{LP}_{11}$  mode is aligned with the  $y$  axis as in Fig. 119.16(c). This orientation of  $\text{LP}_{11}$  produces degradation of  $M^2$  that is more severe in the  $y$  direction. The value of  $M_y^2$  depends on the relative phase between the modes.<sup>3</sup>

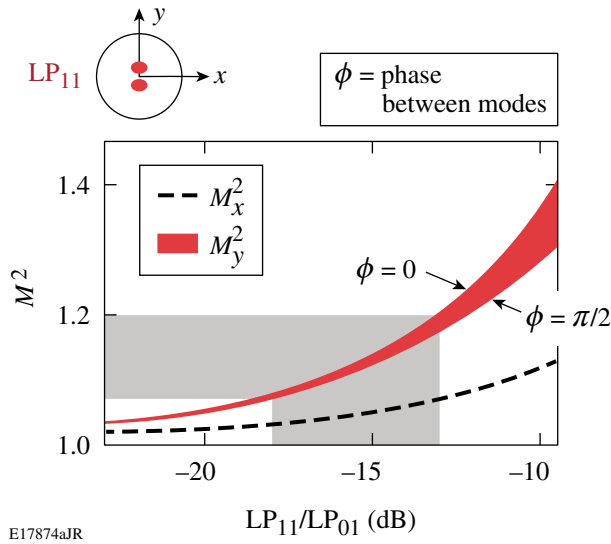


Figure 119.20

Simulations using a simple step-index model showing the impact  $\text{LP}_{11}$  content can have on the beam quality  $M^2$ . Results are shown along both  $x$  and  $y$  directions as a function of relative power of  $\text{LP}_{11}$  and  $\text{LP}_{01}$  modes. The  $M^2$  degradation is more severe along the  $y$  direction (the axis of the  $\text{LP}_{11}$  mode) and depends on the relative phase  $\phi$  between the modes. The grey region shows the range of  $\text{LP}_{11}$  content measured in the PCF amplifier and the corresponding range of  $M^2$  values predicted by this simple model.

Measurements of  $M^2$  show degradation when the amount of  $\text{LP}_{11}$  is increased by misaligning the signal at injection (see Fig. 119.21). The largest increase occurs in  $M_y^2$  (as predicted by the simulations) and when the injection offset is along the  $y$  axis (as predicted by the  $S^2$  measurements). This is consistent with the fact that this offset direction produces the largest amount of  $\text{LP}_{11}$ .  $M^2$  degradation from  $x$ -axis offsets cannot be explained by the level of  $\text{LP}_{11}$  alone. It is likely that other higher-order leaky modes or spatially incoherent scattering within the amplifier that is not resolved in the  $S^2$  measurements but can degrade  $M^2$  are responsible.

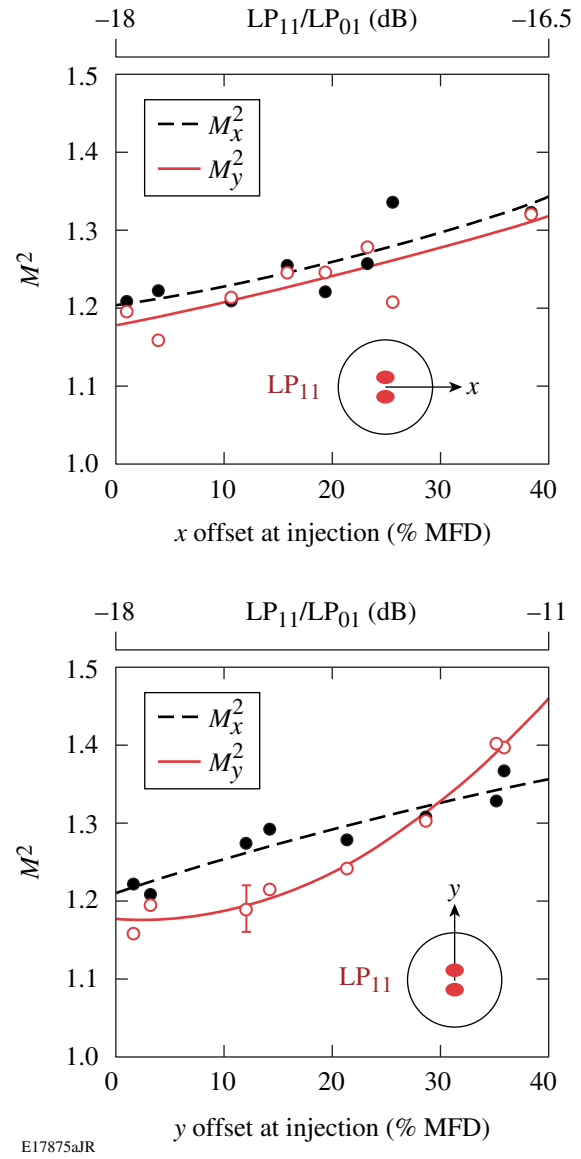


Figure 119.21

Measured  $M^2$  for injection offsets. Offset in the (a)  $x$  direction and (b)  $y$  direction. Inset shows the offset direction relative to the orientation of the  $\text{LP}_{11}$  mode.

In conclusion,  $S^2$  imaging has been used for the first time to measure higher-order mode content of a large-mode-area amplifier at full power. Minor modifications to the technique were necessary to accommodate the short amplifier length and small relative group delay. An HOM corresponding to the co-polarized  $\text{LP}_{11}$  mode was clearly observed with an axis aligned to the birefringent axis of the polarizing amplifier. The power in the  $\text{LP}_{11}$  mode relative to the fundamental  $\text{LP}_{01}$  mode depended on the alignment of the signal at injection. A relative power of

−18 dB was measured when optimally aligned.  $LP_{11}$  content increased when the injected beam was offset, particularly when the offset direction was toward one of the  $LP_{11}$  lobes. An offset of  $\sim 30\%$  of the  $55\text{-}\mu\text{m}$  MFD increased the  $LP_{11}$  content to −13 dB while only decreasing the amplifier gain by  $\sim 0.5$  dB.

#### ACKNOWLEDGMENT

The authors thank Jeff Nicholson, Ingmar Hartl, and Martin Fermann for helpful discussions. This work was supported by the U.S. Department of Energy Office of Inertial Confinement Fusion under Cooperative Agreement No. DE-FC52-08NA28302, the University of Rochester, and the New York State Energy Research and Development Authority. The support of DOE does not constitute an endorsement by DOE of the views expressed in this article.

#### REFERENCES

1. F. Röser *et al.*, Opt. Lett. **32**, 3495 (2007).
2. O. Schmidt *et al.*, Opt. Express **16**, 3918 (2008).
3. H. Yoda, P. Polynkin, and M. Mansuripur, J. Lightwave Technol. **24**, 1350 (2006).
4. S. Wielandy, Opt. Express **15**, 15,402 (2007).
5. J. W. Nicholson *et al.*, Opt. Express **16**, 7233 (2008).
6. J. W. Nicholson *et al.*, IEEE J. Sel. Top. Quantum Electron. **15**, 61 (2009).